POLITECNICO DI TORINO
Repository ISTITUZIONALE

Massive quantum vortices in superfluids

(Article begins on next page)

12 May 2024

PAPER • OPEN ACCESS

Massive Quantum Vortices in Superfluids

To cite this article: Andrea Richaud *et al* 2023 *J. Phys.: Conf. Ser.* **2494** 012016

View the article online for updates and enhancements.

Massive Quantum Vortices in Superfluids

Andrea Richaud

Scuola Internazionale Superiore di Studi Avanzati (SISSA), Via Bonomea 265, I-34136, Trieste, Italy

Departament de Física, Universitat Politècnica de Catalunya, Campus Nord B4-B5, E-08034 Barcelona, Spain

E-mail: `andrea.richaud@upc.edu`

Vittorio Penna

Dipartimento di Scienza Applicata e Tecnologia and u.d.r. CNISM, Politecnico di Torino, Corso Duca degli Abruzzi 24, I-10129 Torino, Italy

Alexander L. Fetter

Departments of Physics and Applied Physics, Stanford University, Stanford, CA 94305-4045, USA

Abstract. We consider the dynamical properties of quantum vortices with filled massive cores, hence the term "massive vortices". While the motion of massless vortices is described by first-order motion equations, the inclusion of core mass introduces a second-order time derivative in the motion equations and thus doubles the number of independent dynamical variables needed to describe the vortex. The simplest possible system where this physics is present, i.e. a single massive vortex in a circular domain, is thoroughly discussed. We point out that a massive vortex can exhibit various dynamical regimes, as opposed to its massless counterpart, which can only precess at a constant rate. The predictions of our analytical model are validated by means of numerical simulations of coupled Gross-Pitaevskii equations, which indeed display the signature of the core inertial mass. Eventually, we discuss a nice formal analogy between the motion of massive vortices and that of massive charges in two-dimensional domains pierced by magnetic fields.

1. Introduction

The dynamics of quantum vortices in superfluids has been a vivid research field ever since 1955, when Feynman published his seminal article [1] about the quantum properties of liquid Helium. The appearance of these topological excitations in a quantum fluid, in fact, constitutes a signature of its superfluid character, i.e. of the presence of a macroscopic wavefunction associated to the system [2]. Originally, their observation was limited to superfluid Helium (see Ref. [3] and references therein), but, following the experimental realization of Bose-Einstein condensation of ultracold atomic gases [4, 5], quantum vortices started to be observed also in this new class of superfluid systems [6, 7, 8, 9, 10]. At present, considerable attention is devoted to the experimental observation of the real dynamics of few-vortex systems [11, 12, 13].

Typically, the Helmholtz-Kirchhoff equations governing the motion of quantum vortices in quasi two-dimensional (2D) domains do not include any inertial term, and the resulting

dynamical equations are first-order differential equations. This implies that the velocity of each vortex depends only on the position of the other vortices in the system and constitutes a profound difference with respect to the well-known Newton's law of motion, according to which the motion of massive particles is governed by second-order differential equations.

Recently, we suggested that, whenever the vortex core hosts massive particles (for which, in turn, the vortex core constitutes a potential well), the resulting composite object eludes the standard description in terms of first-order-differential equations. The presence of a non-zero core mass, in fact, introduces a second-order time derivative in the motion equations and thus doubles the number of independent dynamical variables which can be associated to each vortex. Within a time-dependant variational approximation scheme, we derived an effective point-like dynamical model [14, 15, 16] which accounts for Superfluid Vortex Dynamics and Newtonian Dynamics on equal footing, and which can be applied to both uniform [14, 15] and non-uniform [16] background condensate densities. In particular, in the latter reference, we extended the results of Refs. [17, 18, 19, 20] to the case of a generic power-law trapping potential $\propto r^k$ and to the case of a non-zero core mass. Indeed, the presence of a massive core resulted in a number of intriguing dynamical regimes, including, but not limited to, the occurrence of small-amplitude transverse radial oscillations superimposed to the well-known vortices trajectories [15], and the reversal of the precession direction [16]. The predictions of our analytical model are confirmed by extensive numerical simulations of time-dependent Gross-Pitaevskii (GP) equations for realistic two-component BECs.

The outline of the manuscript is the following: in sections 2 and 3, we review standard analytical techniques for the study of the dynamics of massless vortices. In section 4, we present the effective Lagrangian and the dynamical regimes associated to a single massive superfluid vortex in a circular domain, while in section 5 we focus on two-massive-vortex systems. Section 6 highlights the formal analogy between the motion equations of massive vortices and that of massive charges in quasi-2D domains pierced by a transverse magnetic field. Section 7 includes the results of time-dependent GP simulations, which validate the predictions of the analytical model. Eventually, section 8 is devoted to the concluding remarks and sketches some possible future research directions.

2. Superfluid vortex dynamics

The state of a superfluid system is typically described in terms of a macroscopic wavefunction $\psi = \sqrt{n} e^{i\theta}$, where n and θ are the density and the phase fields respectively. If the system can be considered incompressible (this is typically the case of superfluid ^{4}He and atomic BECs in the strongly interacting Thomas-Fermi regime), the spatial variations of n can be neglected.

The nonviscous, incompressible, and irrotational flow associated to such superfluids can be associated, for quasi-2D systems, to the complex potential

$$F(z) = \chi(\boldsymbol{r}) + i\theta(\boldsymbol{r}) \tag{1}$$

where $\boldsymbol{r} = (x, y)$ and $z = x + iy$. The real part of the complex potential, $\chi(\boldsymbol{r})$, represents the stream function, while the imaginary part, $\theta(\boldsymbol{r})$, corresponds to the velocity potential. Both quantities are strictly linked to the velocity field $\boldsymbol{v}(\boldsymbol{r})$ of the flow by means of the following relations:

$$\boldsymbol{v} = -\frac{\hbar}{m}\nabla \times (\hat{z}\chi), \tag{2}$$

$$\boldsymbol{v} = \frac{\hbar}{m}\nabla\theta. \tag{3}$$

The equivalence between the two descriptions can be understood by recalling that the complex derivative

$$F'(z) = \frac{\partial \chi}{\partial x} + i\frac{\partial \theta}{\partial x} = \frac{\partial \theta}{\partial y} - i\frac{\partial \chi}{\partial y} \tag{4}$$

is characterized by the well-known Cauchy-Riemann conditions

$$\frac{\partial \theta}{\partial x} = -\frac{\partial \chi}{\partial y}, \qquad \frac{\partial \theta}{\partial y} = +\frac{\partial \chi}{\partial x} \tag{5}$$

due to its analytic properties. We remark that the possibility to write $\boldsymbol{v}$ as the *gradient* of a (scalar) velocity potential ensures that the flow is irrotational ($\nabla \times \boldsymbol{v} = \boldsymbol{0}$), apart from singularities corresponding to vortex cores, while the description in terms of the stream function χ ensures that $\boldsymbol{v}$ is incompressible ($\nabla \cdot \boldsymbol{v} = 0$).

Equations (2), (3) and (4) imply that $F'(z) = (m/\hbar)(v_y + iv_x)$. In particular, the complex velocity of a vortex at a point z_0 is given by

$$i\dot{z}_0^* = \dot{y}_0 + i\dot{x}_0 = \frac{\hbar}{m} \lim_{z \to z_0} \left[F'(z) - \frac{1}{z - z_0} \right], \tag{6}$$

where z_0^* is the complex conjugate of z_0 and the term $-1/(z - z_0)$ removes the (diverging) self-contribution of the considered vortex from the overall velocity field [21]. The scope of this formula is rather broad, as it can be used to obtain the motion equations of each vortex present in the system. Notice that such equations are *first-order* ordinary differential equations, in stark contrast to *second-order* Newton equations which are well-known to model the dynamics of massive objects.

3. A massless vortex in a circular domain

Let us consider a vortex at position $\boldsymbol{r}_0 = (x_0, y_0)$ in an incompressible superfluid confined in a circular trap of radius R centered at the origin. The complex potential associated to this problem reads

$$F(z) = \log\left(\frac{z - z_0}{z - z_0'} \right) \tag{7}$$

with $z_0 = x_0 + iy_0$ and $z_0' = x_0' + iy_0'$, where

$$x_0' = \frac{R^2}{x_0^2 + y_0^2} x_0, \qquad y_0' = \frac{R^2}{x_0^2 + y_0^2} y_0 \tag{8}$$

are the coordinates of the image vortex, a fictitious vortex which originates due to the presence of the boundary and which ensures that the overall velocity field $\boldsymbol{v}$ is purely tangent to the boundary itself (i.e. to the circle $x^2 + y^2 = R^2$). Straightforward computations allow one to compute the stream function

$$\chi(\boldsymbol{r}) = \text{Re}(F) = \log\left| \frac{\boldsymbol{r} - \boldsymbol{r}_0}{\boldsymbol{r} - \boldsymbol{r}_0'} \right| \tag{9}$$

and the phase field

$$\theta(\boldsymbol{r}) = \text{Im}(F) = \arctan\left(\frac{y - y_0}{x - x_0} \right) - \arctan\left(\frac{y - y_0'}{x - x_0'} \right) \tag{10}$$

whose plots are illustrated in Fig. 1.

A direct application of formula (6) allows one to determine the motion equation for the vortex, which can be written, in compact form, as

$$\dot{\boldsymbol{r}}_0 = \hat{z} \times \frac{\hbar}{m} \frac{\boldsymbol{r}_0}{R^2 - r_0^2}. \tag{11}$$
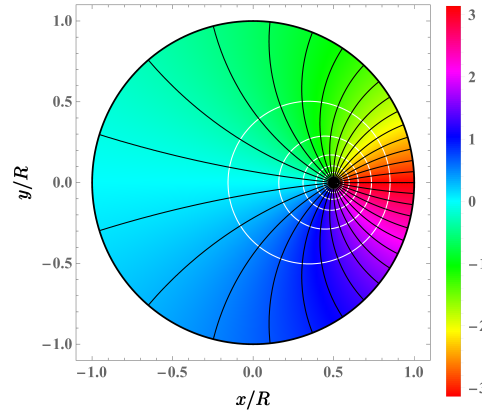
Figure 1. Phase field associated to a vortex in a circular domain of radius R. The vortex is at position $\boldsymbol{r}_0/R = (x_0, y_0)/R = (0.5, 0)$. Black lines are constant-phase lines [see equation (10)], while white circles are streamlines, i.e. lines along which $\chi(\boldsymbol{r})$ [see equation (9)] is constant. The phase ranges from $-\pi$ to π, as visible in the color bar.

That of the complex potential constitutes a very powerful analytical framework for the study of superfluid vortex dynamics and its remarkable "elegance" originates from the link with the theory of analytic functions. Yet, this elegance is associated with an intrinsic rigidity, meaning that such framework is not suitable to incorporate the inertial effect ensuing from the possible presence of core mass. In view of this generalization (which will be describes in section 4 as suitable), we present here an alternative approach which goes under the name of "Time Dependent Variational Lagrangian" [22, 23, 15]. One starts from the customary Gross-Pitaevskii field Lagrangian

$$\mathcal{L}[\psi] = \mathcal{T}[\psi] - \mathcal{E}[\psi] \tag{12}$$

where

$$\mathcal{T}[\psi] = \frac{i\hbar}{2} \int \left(\psi^*(\boldsymbol{r},t) \frac{\partial \psi(\boldsymbol{r},t)}{\partial t} - \frac{\partial \psi^*(\boldsymbol{r},t)}{\partial t} \psi(\boldsymbol{r},t) \right) \mathrm{d}^2 r, \tag{13}$$

$$\mathcal{E}[\psi] = \int \left(\frac{\hbar^2}{2m} |\nabla \psi(\boldsymbol{r},t)|^2 + V_{\mathrm{tr}} |\psi(\boldsymbol{r},t)|^2 + \frac{g}{2} |\psi(\boldsymbol{r},t)|^4 \right) \mathrm{d}^2 r \tag{14}$$

(see section 7 for the detailed meaning of the various parameters) and makes a time-dependent variational ansatz, in this case

$$\psi = \sqrt{n} e^{i\theta} \tag{15}$$

where the density field n is uniform in the region $x^2 + y^2 < R^2$ except for the region $(\boldsymbol{r}-\boldsymbol{r}_0)^2 < \xi^2$ where it is zero (ξ is a cut-off length-scale introduced to ensure the convergence of the integrals) and the phase field is given by equation (10). Then one substitutes this time-dependent variational ansatz into field Lagrangian (12) and, upon integrating away the field degrees of freedom and neglecting constant terms, obtains an effective classical Lagrangian which depends only on the position $\boldsymbol{r}_0$ and on the velocity $\dot{\boldsymbol{r}}_0$ of the vortex:

$$L = \hbar n\pi (\dot{\boldsymbol{r}}_0 \times \boldsymbol{r}_0 \cdot \hat{z}) \frac{r_0^2 - R^2}{r_0^2} - \frac{\hbar^2 n\pi}{m} \log\left(1 - \frac{r_0^2}{R^2}\right). \tag{16}$$

One has thus reduced the original problem to that of a point particle. Notice, in passing, that Lagrangian (16) may be found under different, but equivalent, forms (see, for example, Refs.

[15, 16]) differing due to a total time derivative. The ensuing Euler-Lagrange motion equation is independent of this specific "gauge choice" and reads

$$\mathbf{0} = \hat{z} \times \dot{\boldsymbol{r}}_0 + \frac{\hbar}{m} \frac{\boldsymbol{r}_0}{R^2 - r_0^2} \tag{17}$$

and manifestly coincides with the one previously determined within the complex-potential framework [see equation (11)]. It is clear that equation (17) corresponds to a uniform circular motion whose center is the point $(0,0)$, whose radius is r_0 and whose precession rate is

$$\Omega_0 = \frac{\hbar}{m(R^2 - r_0^2)}. \tag{18}$$

4. Introduction of core mass

The presence of massive particles trapped in the vortex core can be incorporated in the Lagrangian model. In Refs. [14], [15] and [16] these particles were assumed to constitute a different BEC. The latter can be described in terms of a Gaussian wavefunction

$$\psi_b = \sqrt{\frac{N_b}{\pi \sigma^2}} e^{-\frac{|\boldsymbol{r} - \boldsymbol{r}_0(t)|^2}{2\sigma^2}} e^{i\boldsymbol{r} \cdot \boldsymbol{\alpha}_0(t)} \tag{19}$$

[where N_b is the number of component-b atoms, σ is the typical width of Gaussian and $\boldsymbol{\alpha}_0$ is a time-dependent variational parameter which allows for non-zero translational velocities $\dot{\boldsymbol{r}}_0 = (m_b/\hbar)\boldsymbol{\alpha}_0$], or super-Gaussian functions [24], while in Ref. [25] they were classical objects (mimicking tracer particles used as vorticity tracers in liquid-Helium experiments). Regardless of the microscopic origin of these core-filling particles, as long as they stay tightly trapped in the vortex core, their effective Lagrangian is

$$L_b = \frac{1}{2} M_b \dot{\boldsymbol{r}}_0^2 \tag{20}$$

where $M_b = N_b m_b$ is their total mass (m_b being the component-b atomic mass). Notice the use of the *same* dynamical variable $\boldsymbol{r}_0$ to denote both the position of the vortex in ψ_a and that of the component-b inertial particles, an approximation justified by the assumed immiscibility of the two components. The total Lagrangian associated to these "massive vortices" can be therefore written as

$$L = L_a + L_b \tag{21}$$

where L_a corresponds to Lagrangian (16) and L_b to Lagrangian (20). Notice that, due to the rotational invariance of the system, the (third component of the) angular momentum

$$L_z = (\boldsymbol{r}_0 \times \boldsymbol{p}_0) \cdot \hat{z} = n_a \pi \hbar (R^2 - r_0^2) + M_b (\boldsymbol{r}_0 \times \dot{\boldsymbol{r}}_0) \cdot \hat{z} \tag{22}$$

constitutes a conserved quantity ($\boldsymbol{p}_0 = \partial L / \partial \dot{\boldsymbol{r}}_0$ represents the canonical momentum).

The Euler-Lagrange motion equation associated to Lagrangian (21) reads:

$$M_b \ddot{\boldsymbol{r}}_0 = 2 n_a \pi \hbar \left[\hat{z} \times \dot{\boldsymbol{r}}_0 + \frac{\hbar}{m_a} \frac{\boldsymbol{r}_0}{R^2 - r_0^2} \right] \tag{23}$$

where we have introduced the subscript "a" to quantities associated to the wavefunction featuring the vortex. Notice that, as opposed to equations (6) and (11), equation (23) is manifestly a *second-order* differential equation. This constitutes a remarkable difference, as the presence of mass effectively *doubles* the number of independent dynamical variables associated
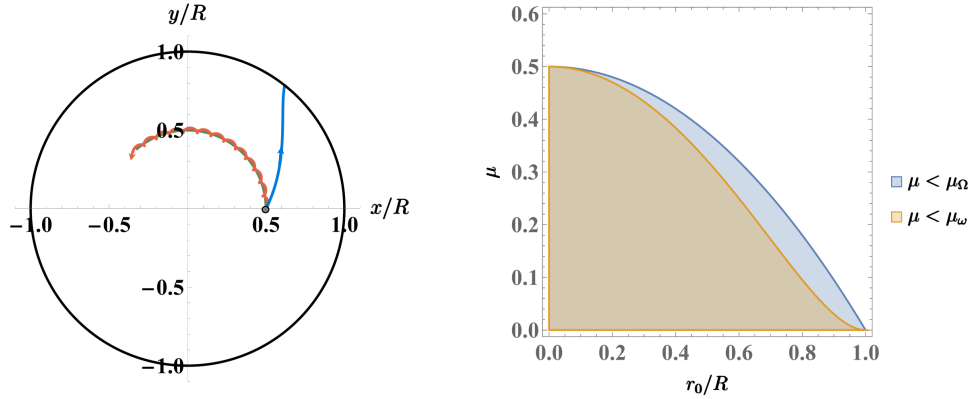
Figure 2. Left panel: three possible trajectories for a massive vortex in a circular trap. Green curve is obtained for the initial conditions $\boldsymbol{r}_0(0)/R = (0.5, 0)$ and $\dot{\boldsymbol{r}}_0(0) = (0, r_0\Omega_0^{(-)})$, where $\Omega_0^{(-)}$ is the dimensionful version of equation (26), red curve is obtained for small perturbations of the initial conditions. In both cases, $\mu = 4 \times 10^{-2}$. For larger values of the core mass, inequalities (27) and (35) may be violated and the insuing dynamical instability results in a collision with the circular boundary (see the blue line, obtained for $\mu = 0.5$). Right panel: plot of inequalities (27) and (35). The uniform circular orbits exist and are dynamically stable in the common region, i.e. for $\mu < \mu_\omega$.

to the system. It it worth mentioning that equation (23) has the classic form of a singular perturbation, with the small parameter M_b multiplying the highest derivative.

Equation (23) features some notable dynamical regimes (see, e.g., the left panel of Fig. 2). One of them is represented by uniform circular orbits, i.e. solutions of the type:

$$\boldsymbol{r}_0(t) = r_0\ (\cos(\Omega_0 t),\ \sin(\Omega_0 t)) \tag{24}$$

where the precession frequency Ω_0 depends both on the radial position r_0 and on the core mass M_b. Introducing, for convenience, the dimensionless quantities $\tilde{r}_0 := r_0/R$, $\tilde{\Omega}_0 := \Omega_0/[\hbar/(m_a R^2)]$, and $\mu = M_b/M_a = (N_b m_b)/(N_a m_a) = (N_b m_b)/(n_a \pi R^2 m_a)$, two solutions are possible [15]:

$$\tilde{\Omega}_0^{(+)} = \frac{1 + \sqrt{1 - 2\mu/(1 - \tilde{r}_0^2)}}{\mu} \tag{25}$$

$$\tilde{\Omega}_0^{(-)} = \frac{2/(1 - \tilde{r}_0^2)}{1 + \sqrt{1 - 2\mu/(1 - \tilde{r}_0^2)}}. \tag{26}$$

Notice that, in the limit of vanishingly small core mass (i.e. for $\mu \to 0$), $\tilde{\Omega}_0^{(+)}$ diverges as $\sim 2/\mu$ and thus becomes unphysical, while $\tilde{\Omega}_0^{(-)} \to 1/(1 - \tilde{r}_0^2)$, which indeed corresponds to precession rate (18) when written in dimensionful form. We remark that uniform circular orbits exist provided that the core mass is sufficiently small, i.e. for

$$\mu < \mu_\Omega := \frac{1}{2}(1 - \tilde{r}_0^2). \tag{27}$$

To study the dynamical stability of these uniform circular orbits, one begins with moving from the lab frame xOy to a new reference frame $x'Oy'$ rotating at frequency Ω_0 with respect to the previous one. The transformation is given by

$$x_0 = x_0' \cos(\Omega_0 t) - y_0' \sin(\Omega_0 t), \qquad y_0 = x_0' \sin(\Omega_0 t) + y_0' \cos(\Omega_0 t) \tag{28}$$

(of course, the velocities transform accordingly). In this rotating frame the vortex coordinates read $\boldsymbol{r}_0' := (x_0', y_0')$ and the Lagrangian can be written as

$$L' = L(\boldsymbol{r}_0', \, \dot{\boldsymbol{r}}_0') + \Omega_0 L_z(\boldsymbol{r}_0', \, \dot{\boldsymbol{r}}_0') + \frac{1}{2}M_b\Omega_0^2 r_0'^{\,2} \tag{29}$$

where $L(\boldsymbol{r}_0', \, \dot{\boldsymbol{r}}_0')$ and $L_z(\boldsymbol{r}_0', \, \dot{\boldsymbol{r}}_0')$ correspond to equations (21) and (22), respectively, but now with all the original (unprimed) laboratory dynamical variables replaced by those in the (primed) rotating frame. In this reference frame, the previously discussed uniform circular orbits (24) constitute fixed points.

Performing the Legendre transform, one can easily prove that the Hamiltonian associated to Lagrangian (29) reads

$$H' = H(\boldsymbol{r}_0', \, \boldsymbol{p}_0') - \Omega_0 L_z(\boldsymbol{r}_0', \, \boldsymbol{p}_0') \tag{30}$$

where H is the Hamiltonian associated to Lagrangian (21), i.e.

$$H(\boldsymbol{r}_0, \, \boldsymbol{p}_0) = \frac{(\boldsymbol{p}_0 - k\boldsymbol{A})^2}{2M_b} - \frac{n_a^2\pi^2R^2\hbar^2}{M_b}\left(1 - \frac{R^2}{2r_0^2}\right) - \frac{n_a\pi R^2\hbar}{M_b}\frac{\boldsymbol{r}_0 \times \boldsymbol{p}_0}{r_0^2}\cdot\hat{z} + \frac{\hbar^2 n_a\pi}{m_a}\log\left(1 - \frac{r_0^2}{R^2}\right) \tag{31}$$

but with all original laboratory canonical variables replaced by those in the rotating frame [we have introduced the symbols $k = h/m_a$, and $\boldsymbol{A} := m_a n_a(y_0, \, -x_0)/2$, the latter being an effective vector potential which corresponds to an effective synthetic gauge field [15, 16]]. After defining the vector $\boldsymbol{v}' = (\boldsymbol{r}_0', \, \boldsymbol{p}_0')$ of canonical variables in the rotating frame, it is straightforward to verify that the set of Hamilton equations $\dot{\boldsymbol{v}}' = \mathcal{E}\nabla H'$, where $\mathcal{E}$ is the standard symplectic matrix, admits a class of fixed points $\boldsymbol{v}^{*\prime}$ corresponding to uniform circular motions (24) in the lab frame. As is well known from Dynamical-System Theory, the fixed point is stable provided that the eigenvalues of the corresponding Jacobian matrix

$$\mathcal{J}(\boldsymbol{v}^{*\prime}) = \mathcal{E}\mathcal{H}|_{\boldsymbol{v}'=\boldsymbol{v}^{*\prime}} \tag{32}$$

where $\mathcal{H} := (\partial^2 H')/(\partial v_i'\partial v_j')$ is the Hessian matrix associated to Hamiltonian (30), have no (positive) real part. Lengthy but straightforward computations lead to the four eigenvalues

$$\lambda_1 = 0, \qquad \lambda_2 = 0, \qquad \lambda_3 = +i\omega, \qquad \lambda_4 = -i\omega \tag{33}$$

where

$$\omega = \frac{\hbar}{m_aR^2}\frac{2}{\mu}\sqrt{1 - \mu\frac{2 - \tilde{r}_0^2}{(1 - \tilde{r}_0^2)^2}}. \tag{34}$$

It worth mentioning that the occurrence of two zero eigenvalues is due to the presence of a conserved quantity, namely L_z, or, in other words, to the fact that all the points lying on the circumference $r_0' = \text{const}$ constitute equivalent fixed points. One can readily verify that eigenfrequency (34) is real provided that

$$\mu < \mu_\omega := \frac{(1 - \tilde{r}_0^2)^2}{2 - \tilde{r}_0^2}. \tag{35}$$

The same results can be obtained by studying the effective potential associated to the motion along the radial direction [15, 16]. The plot of inequality (27) and inequality (35) is illustrated in the right panel of Fig. 2, which clearly shows that, for this system, if a uniform circular motion exists, than it is also dynamically stable.

5. Two-massive-vortex systems

The arguments developed in sections 3 and 4 can be easily generalized to the case of many-vortex systems. In this section, we focus on *two*-vortex systems. In the massless case, the dynamics of two-vortex systems confined in 2D circular domains can be completely determined within the complex-potential framework. One starts from

$$F(z) = q_1 \log \left(\frac{z - z_1}{z - z_1'} \right) + q_2 \log \left(\frac{z - z_2}{z - z_2'} \right) \tag{36}$$

where q_1 and q_2 can take the values ± 1, z_1 and z_2 are the positions of the two real vortices, and z_1' and z_2' are the positions of their images [see equation (8)], and uses formula (6) to determine the motion of each vortex (notice that one obtains *first-order* differential equations). Figure 3 illustrates the phase field and the streamlines associated to this system in the case of same-signed vortices (left panel) and opposite-signed vortices (right panel).
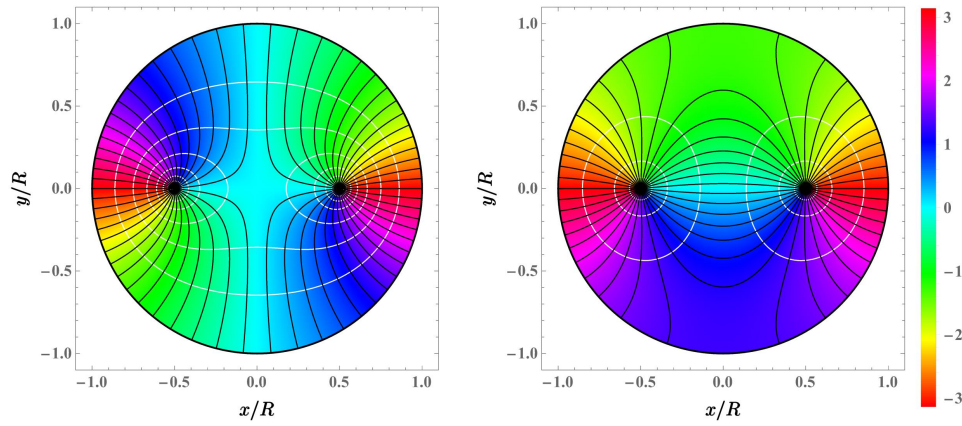

Figure 3. Phase field associated to two-vortex states in a circular domain of radius R. Left (right) panel corresponds to same-signed (opposite-signed) vortices. In both cases, vortices are at position $\boldsymbol{r}_1/R = -\boldsymbol{r}_2/R = (0.5, 0)$. Black lines are constant-phase lines, while white circles are streamlines, i.e. lines along which $\chi(\boldsymbol{r})$ is constant. The phase ranges from $-\pi$ to π, as visible in the color bar.

As already mentioned, the presence of core mass and the inertial effects it comes with cannot be incorporated in this description. It is indeed preferable to develop the Time-Dependent-Variational-Lagrangian scheme. Following the same steps described in sections 3 and 4, one can write the effective point-like Lagrangian associated to the system

$$L = \sum_{j=1}^{2} \left(\frac{M_{b,j}}{2} \dot{\boldsymbol{r}}_j^2 \right) + \sum_{j=1}^{2} \left[\frac{q_j k m_a n_a}{2} (\dot{\boldsymbol{r}}_j \times \boldsymbol{r}_j \cdot \hat{z}) \frac{r_j^2 - R^2}{r_j^2} - \frac{m_a n_a k^2}{4\pi} \log \left(1 - \frac{r_j^2}{R^2} \right) \right] - V(\boldsymbol{r}_1, \boldsymbol{r}_2) \tag{37}$$

where

$$V = \frac{m_a n_a k^2}{4\pi} q_1 q_2 \ln \left(\frac{R^2 - 2\boldsymbol{r}_1 \cdot \boldsymbol{r}_2 + r_1^2 r_2^2/R^2}{r_1^2 - 2\boldsymbol{r}_1 \cdot \boldsymbol{r}_2 + r_2^2} \right) \tag{38}$$

is the two-vortex interaction term.

The relevant Euler-Lagrange motion equations read

$$M_{b,j} \ddot{\boldsymbol{r}}_j = q_j k m_a n_a \hat{z} \times \dot{\boldsymbol{r}}_j + m_a n_a \frac{k^2 q_j}{2\pi} \left[q_i \frac{\boldsymbol{r}_j - \boldsymbol{r}_i}{|\boldsymbol{r}_j - \boldsymbol{r}_i|^2} + q_j \frac{\boldsymbol{r}_j}{R^2 - r_j^2} + q_i \frac{R^2 \boldsymbol{r}_i - r_i^2 \boldsymbol{r}_j}{R^4 - 2R^2 \boldsymbol{r}_i \boldsymbol{r}_j + r_i^2 r_j^2} \right] \tag{39}$$

and they can be conveniently used to obtain the vortices' trajectories (see, e.g., Sec. III.B of Ref. [15]).

6. Electromagnetic equivalence

The equations describing the motion of massive vortices are formally equivalent to the ones describing the motion of massive charges in 2D domains pierced by magnetic fields. To explicitly show this nice mapping, we rewrite motion equation (23) as

$$M_b \ddot{\boldsymbol{r}}_0 = k \dot{\boldsymbol{r}}_0 \times (-m_a n_a \hat{z}) + \frac{m_a n_a}{2\pi} k k' \frac{\boldsymbol{r}_0 - \boldsymbol{r}_0'}{|\boldsymbol{r}_0 - \boldsymbol{r}_0'|^2} \tag{40}$$

[where $k = (+1)h/m_a$, $\boldsymbol{r}_0' = \boldsymbol{r}_0 R^2/r_0^2$ is the position of the image vortex, and $k' = -k$ its strength] and motion equations (39) as

$$M_{b,1} \ddot{\boldsymbol{r}}_1 = k_1 \dot{\boldsymbol{r}}_1 \times (-m_a n_a \hat{z}) + \frac{m_a n_a}{2\pi} \left[k_1 k_1' \frac{\boldsymbol{r}_1 - \boldsymbol{r}_1'}{|\boldsymbol{r}_1 - \boldsymbol{r}_1'|^2} + k_1 k_2 \frac{\boldsymbol{r}_1 - \boldsymbol{r}_2}{|\boldsymbol{r}_1 - \boldsymbol{r}_2|^2} + k_1 k_2' \frac{\boldsymbol{r}_1 - \boldsymbol{r}_2'}{|\boldsymbol{r}_1 - \boldsymbol{r}_2'|^2} \right] \tag{41}$$

$$M_{b,2} \ddot{\boldsymbol{r}}_2 = k_2 \dot{\boldsymbol{r}}_2 \times (-m_a n_a \hat{z}) + \frac{m_a n_a}{2\pi} \left[k_2 k_2' \frac{\boldsymbol{r}_2 - \boldsymbol{r}_2'}{|\boldsymbol{r}_2 - \boldsymbol{r}_2'|^2} + k_2 k_1 \frac{\boldsymbol{r}_2 - \boldsymbol{r}_1}{|\boldsymbol{r}_2 - \boldsymbol{r}_1|^2} + k_2 k_1' \frac{\boldsymbol{r}_2 - \boldsymbol{r}_1'}{|\boldsymbol{r}_2 - \boldsymbol{r}_1'|^2} \right] \tag{42}$$

where $k_j = q_j k$, and $q_j \in \{-1, +1\}$. These equations are manifestly formally equivalent to Newton second law $M_{b,j} \ddot{\boldsymbol{r}}_j = \boldsymbol{F}_j$ for a particle of mass $M_{b,j}$ and "charge" k_j in an electromagnetic field. The force $\boldsymbol{F}_j$ applied on the j-th vortex, in fact, can be regarded as the sum of two contributions: a Lorentz-like force $k_j \dot{\boldsymbol{r}}_j \times (-m_a n_a \hat{z})$ which is perpendicular to the vortex velocity $\dot{\boldsymbol{r}}_j$ (and hence does not do work), and a Coulomb-like force $k_j \boldsymbol{E}(\boldsymbol{r}_j)$, where $\boldsymbol{E}(\boldsymbol{r}_j)$ can be regarded as the superposition of the "electric fields" generated by all the remaining "charges" (be them real or virtual) present in the system. We remark that, as opposed to the familiar Coulomb force in standard electrostatic problems, which decays as r_{12}^{-2} (where r_{12} is the inter-vortex distance), in the present case the Coulomb-like force decays as r_{12}^{-1} because of the reduced dimensionality of the system. We also recall that one should write the motion equations only for *real* vortices, i.e. the ones associated to *unprimed* variables $\boldsymbol{r}_j$ and $\dot{\boldsymbol{r}}_j$. The *image* vortices, instead, do not have an independent dynamics, their position being determined, at any time, by equation (8). Within this formal analogy, the superfluid density $m_a n_a$ constitutes (the magnitude of) an effective magnetic field [$\boldsymbol{B} := -m_a n_a \hat{z} = \nabla \times \boldsymbol{A}$, where the vector potential $\boldsymbol{A}$ was introduced in Hamiltonian (31)] which pierces the plane on which vortices move, while the inter-vortex interactions (as well as the possible presence of geometric boundaries) result in an effective electric field.

7. Massive quantum vortices in two-component BECs

In this section, we benchmark the predictions of motion equation (23) against numerical simulations of couple GP equations

$$i\hbar \frac{\partial \psi_a}{\partial t} = \left[-\frac{\hbar^2}{2m_a} \nabla^2 + V_{\text{tr}} + g_{aa} |\psi_a|^2 + g_{ab} |\psi_b|^2 \right] \psi_a \tag{43}$$

$$i\hbar \frac{\partial \psi_b}{\partial t} = \left[-\frac{\hbar^2}{2m_b} \nabla^2 + V_{\text{tr}} + g_{ab} |\psi_a|^2 + g_{ab} |\psi_a|^2 \right] \psi_b, \tag{44}$$

where $\psi_a = \sqrt{n_a} e^{i\theta_a}$ and $\psi_b = \sqrt{n_b} e^{i\theta_b}$ are the macroscopic wavefunctions representing the state the two condensed components (normalized to N_a and N_b, the number of atoms in the two condensed species, respectively), m_a and m_b are the two atomic masses, V_{tr} is the hard-wall

circular confining potential, and $g_{ij} = \sqrt{2\pi}\hbar^2 a_{ij}/(m_{ij}d_z)$ are the intra- and inter-component interactions in 2D. Parameters $m_{ij} = 1/(m_i^{-1} + m_j^{-1})$ represent the effective masses, a_{ij} the intra- and inter-component scattering lengths (typically of the order of tens of Bohr radii $a_0 = 5.29 \times 10^{-11}$ m), and d_z constitutes the effective width of the quasi-2D atomic cloud. The simulations are carried out assuming that component-a (-b) is made up of ^{23}Na (^{39}K) atoms. The scattering lengths are $a_{aa} = 52\,a_0$, $a_{bb} = 7.6\,a_0$ and $a_{ab} = 24.2\,a_0$, implying that $g_{ab}/\sqrt{g_a g_b} \approx 1.3$, so that the immiscibility condition is met, meaning that the component-b core is tightly localized in the component-a vortex.

After generating the initial condition for the real-time dynamics [this is obtained by means of a suitable imaginary-time propagation in a frame rotating at frequency $\Omega_0^{(-)} = \hbar/(m_a R^2)\tilde{\Omega}_0^{(-)}$ [see equation (26)] and then perturbing the phase field of ψ_b so to impose a non-zero radial velocity and thus trigger the small-amplitude radial oscillations], we switched to real-time propagation. The position of the phase singularity and the density minimum in ψ_a is recorded at every iteration. The comparison between this "experimental" trajectory (blue dots) and the one obtained from equation (23) for the same microscopic parameters and initial conditions (red solid line) is shown in Fig. 4. Remarkably, the presence of small-amplitude radial oscillations,
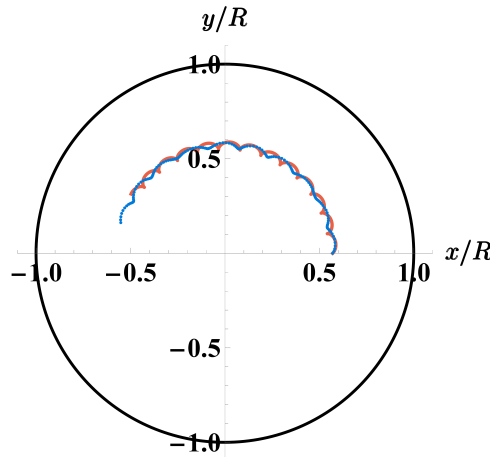

Figure 4. Comparison between the trajectory predicted by equation (23) (red line) and the trajectory extracted from time-dependent GP simulations (blue dots) [see equations (43) and (44)]. We used the following microscopic parameters $N_a = 90 \times 10^3$, $N_b = 2 \times 10^3$ (hence $\mu = 0.04$), $R = 50\,\mu$m. The initial position is at $(x_0, y_0)/R = (0.57, 0)$ and the unperturbed precession frequency reads $\Omega_0^{(-)} = \hbar/(m_a R^2)\tilde{\Omega}_0^{(-)} = 1.68$ rad/s. The ending time of both trajectories is 1.5 s.

which constitute the signature of the inertial effect ensuing from the core mass, is confirmed by our numerical experiments. Yet, from a more quantitative point of view, the *frequency* of these radial oscillations differs from the one predicted by the analytical model. With reference to Fig. 4, one can count ≈ 12.5 cycles as regards the red curve, and ≈ 10 cycles for the blue curve (both trajectories are obtained for the same simulated interval, i.e. $\Delta t = 1.5$ s), corresponding, respectively, to ≈ 52 rad/s and ≈ 42 rad/s. While the first value well corresponds to the one predicted by equation (34), i.e. ≈ 54 rad/s, the second differs of $\approx 20\%$. This difference may be ascribed to a number of phenomena that are indeed present in GP simulations (finite compressibility, emission of sound waves, relative motion between the vortex and its massive core), but are neglected by our analytical model.

8. Conclusions and future perspectives

We have investigated the dynamical properties of quantum vortices with filled massive cores. Traditionally, quantum vortices are regarded as phase singularities with no inertial mass and their motion is typically described by first-order differential equations, meaning that the velocity of each vortex is uniquely determined, at any time, by the positions of all other vortices in the system. The introduction of core mass constitutes a singular perturbation: the number of independent dynamical variables doubles and the motion equations become of second order. We have analyzed, in quiet detail, the simplest possible system where this physics is present, i.e. a massive quantum vortex in a circular region. We have show, in particular, that the presence of inertial mass is responsible for the onset of small-amplitude radial oscillations. This prediction was confirmed by means of numerical simulations of coupled time-dependent GP equations. Eventually, we have pointed out the nice formal analogy between the dynamics of massive quantum vortices and that of massive charges in a 2D domain pierced by a magnetic field.

Possible future research directions include the study of massive-vortex dynamics on curved surfaces, thus generalizing the analysis developed in Refs. [21, 26, 27, 28] to the case of non-zero core mass, the introduction of an inter-component coherent coupling [29, 30] which may result in time-dependant core masses, component-selective potentials [31, 32], dissipation [33], the extension to three-dimensional systems [34, 35] and to miscible components [36, 37, 38]. Also, we are going to investigate the properties of massive-vortex lattices and their associated Tkachenko-like oscillation modes [23]. In this regard, it is worth mentioning that regular arrays of quantum vortices can be regarded as an effective "optical lattice" for the b component, whose quantum properties may be further investigated within an effective (Bose)-Hubbard model [39, 40]. This possible research direction is rather suggestive also in view of the fact that the motion of precession which vortex necklaces are well known to have [23] can be regarded as an effective synthetic gauge field for component-b neutral atoms. Therefore, the wide spectrum of intriguing physical phenomena that are disclosed by Hubbard-like rings pierced by artificial gauge fields [41, 42, 43, 44, 45, 46, 47] may be observed in an optical-lattice-free setup.

References

[1] Feynman R P 1955 *Progress in Low Temperature Physics* vol 1 (Amsterdam: Elsevier, North-Holland) pp 17–53
[2] Zwierlein M W, Abo-Shaeer J R, Schirotzek A, Schunck C H and Ketterle W 2005 *Nature* **435** 1047–1051
[3] Donnelly R J 1991 *Quantized Vortices in Helium II* (Cambridge: Cambridge University Press)
[4] Anderson M H, Ensher J R, Matthews M R, Wieman C E and Cornell E A 1995 *science* **269** 198–201
[5] Davis K B, Mewes M O, Andrews M R, van Druten N J, Durfee D S, Kurn D and Ketterle W 1995 *Phys. Rev. Lett.* **75** 3969
[6] Matthews M R, Anderson B P, Haljan P C, Hall D S, Wieman C E and Cornell E A 1999 *Phys. Rev. Lett.* **83**(13) 2498–2501
[7] Anderson B P, Haljan P C, Wieman C E and Cornell E A 2000 *Phys. Rev. Lett.* **85**(14) 2857–2860
[8] Madison K W, Chevy F, Wohlleben W and Dalibard J 2000 *Phys. Rev. Lett.* **84**(5) 806–809
[9] Abo-Shaeer J R, Raman C, Vogels J M and Ketterle W 2001 *Science* **292** 476–479
[10] Leanhardt A E, Görlitz A, Chikkatur A P, Kielpinski D, Shin Y, Pritchard D E and Ketterle W 2002 *Phys. Rev. Lett.* **89**(19) 190403
[11] Neely T W, Samson E C, Bradley A S, Davis M J and Anderson B P 2010 *Phys. Rev. Lett.* **104**(16) 160401
[12] Serafini S, Galantucci L, Iseni E, Bienaimé T, Bisset R N, Barenghi C F, Dalfovo F, Lamporesi G and Ferrari G 2017 *Phys. Rev. X* **7**(2) 021031
[13] Kwon W J, Del Pace G, Xhani K, Galantucci L, Muzi Falconi A, Inguscio M, Scazza F and Roati G 2021 *Nature* **600** 64–69

[14] Richaud A, Penna V, Mayol R and Guilleumas M 2020 *Phys. Rev. A* **101**(1) 013630

[15] Richaud A, Penna V and Fetter A L 2021 *Phys. Rev. A* **103**(2) 023311

[16] Richaud A, Massignan P, Penna V and Fetter A L 2022 *Phys. Rev. A* **106**(6) 063307

[17] Fetter A L 1998 *Journal of low temperature physics* **113** 189

[18] McGee S A and Holland M J 2001 *Phys. Rev. A* **63**(4) 043608

[19] Ruban V P 2022 *JETP Letters* **115** 415

[20] Katsimiga G C, Mistakidis S I, Mukherjee K, Kevrekidis P G and Schmelcher P 2023 *Phys. Rev. A* **107**(1) 013313

[21] Guenther N E, Massignan P and Fetter A L 2017 *Phys. Rev. A* **96**(6) 063608

[22] Pérez-García V M, Michinel H, Cirac J I, Lewenstein M and Zoller P 1996 *Phys. Rev. Lett.* **77**(27) 5320

[23] Kim J K and Fetter A L 2004 *Phys. Rev. A* **70**(4) 043624

[24] Doran R, Baggaley A and Parker N 2022 *arXiv preprint arXiv:2207.12913*

[25] Griffin A, Shukla V, Brachet M E and Nazarenko S 2020 *Phys. Rev. A* **101**(5) 053601

[26] Massignan P and Fetter A L 2019 *Phys. Rev. A* **99**(6) 063602

[27] Guenther N E, Massignan P and Fetter A L 2020 *Phys. Rev. A* **101**(5) 053606

[28] Caracanhas M A, Massignan P and Fetter A L 2022 *Phys. Rev. A* **105**(2) 023307

[29] Calderaro L, Fetter A L, Massignan P and Wittek P 2017 *Phys. Rev. A* **95**(2) 023605

[30] Choudhury S and Brand J 2022 *Physical Review A* **106** 043319

[31] Richaud A, Lamporesi G, Capone M and Recati A 2022 *arXiv preprint arXiv:2209.00493*

[32] Wang W 2022 *Journal of Physics B: Atomic, Molecular and Optical Physics* **55** 105301

[33] Williamson L A and Blakie P B 2021 *Phys. Rev. Res.* **3**(1) 013154

[34] Ruban V P, Wang W, Ticknor C and Kevrekidis P G 2022 *Physical Review A* **105** 013319

[35] Kasamatsu K, Okada M and Takeuchi H 2023 *Phys. Rev. A* **107**(1) 013309

[36] Gallemí A, Pitaevskii L P, Stringari S and Recati A 2018 *Phys. Rev. A* **97**(6) 063615

[37] Richaud A and Penna V 2019 *Phys. Rev. A* **100**(1) 013609

[38] Penna V and Richaud A 2018 *Scientific Reports* **8** 10242

[39] Chaviguri R H, Comparin T, Bagnato V S and Caracanhas M A 2017 *Phys. Rev. A* **95**(5) 053639

[40] Chaviguri R H, Comparin T, Di Liberto M and Caracanhas M A 2018 *Phys. Rev. A* **97**(2) 023614

[41] Amico L, Anderson D, Boshier M, Brantut J P, Kwek L C, Minguzzi A and von Klitzing W 2022 *Rev. Mod. Phys.* **94**(4) 041001

[42] Naldesi P, Polo J, Dunjko V, Perrin H, Olshanii M, Amico L and Minguzzi A 2022 *SciPost Physics* **12** 138

[43] Chetcuti W J, Haug T, Kwek L C and Amico L 2022 *SciPost Physics* **12** 033

[44] Richaud A, Ferraretto M and Capone M 2021 *Phys. Rev. B* **103**(20) 205132

[45] Pecci G, Naldesi P, Amico L and Minguzzi A 2021 *Physical Review Research* **3** L032064

[46] Amico L, Boshier M, Birkl G, Minguzzi A, Miniatura C, Kwek L C, Aghamalyan D, Ahufinger V, Anderson D, Andrei N *et al.* 2021 *AVS Quantum Science* **3** 039201

[47] Polo J, Naldesi P, Minguzzi A and Amico L 2020 *Phys. Rev. A* **101**(4) 043418